2001

Construction and Reactivity Mapping of a Platinum Catalyst Gradient Using the Scanning Electrochemical Microscope

Shrisudersan Jayaraman, *University of Virginia - Main Campus*
Andrew C. Hillier, *University of Virginia - Main Campus*

Construction and Reactivity Mapping of a Platinum Catalyst Gradient Using the Scanning Electrochemical Microscope

Shrisudersan Jayaraman and Andrew C. Hillier*

Department of Chemical Engineering, University of Virginia, Charlottesville, Virginia 22904

Received June 19, 2001. In Final Form: September 12, 2001

We describe a method for the characterization of electro-oxidation catalysts that involves the fabrication and reactivity mapping of samples possessing a catalyst gradient. The objective of this work is to demonstrate a method for catalyst preparation and screening that directly measures the activity of spatially localized catalyst samples toward electro-oxidation reactions relevant to the fuel cell anode in an effort to discover and characterize new catalyst formulations. In this report, a well-defined gradient in the surface coverage of platinum is created on an electronically conductive but catalytically inactive indium−tin-oxide (ITO) substrate by the application of a nonuniform electric field during platinum electro-deposition. A linear variation in applied potential is imposed on an ITO substrate to induce a nonuniform platinum deposition rate, which results in the formation of a coverage gradient. The reactivity of this catalyst gradient is measured directly as a function of spatial position using a scanning electrochemical microscope in the feedback mode. Surface imaging using a noncatalytic redox couple ($Ru(NH_3)_6^{3+/2+}$) depicts a uniform and highly reactive electrode surface over both ITO and platinum domains. In contrast, imaging with a catalytic probe (H^+/H_2), which senses variations in the substrate activity toward the hydrogen oxidation reaction, clearly illustrates a variation in surface reactivity that is a function of the local substrate composition. The presence of a nonuniform platinum coverage generates a variation in the hydrogen oxidation rate constant. The local reaction rate, as deduced by scanning electrochemical measurements, is proportional to the local platinum surface coverage as determined with electron microscopy. This work demonstrates a unique method for the preparation of catalyst gradient samples coupled with a characterization method that can measure catalytic activity for electro-oxidation reactions on a local scale.

Introduction

The development of fuel cells as high energy density power supplies continues to be the subject of intense research.[1,2] Unfortunately, the performance of many fuel cell systems has not reached competitive levels. Poor performance, as measured by voltage losses in the fuel cell stack, can be attributed to a number of factors, including limitations of anode and cathode as well as losses due to transport limitations across the membrane and in the gas distribution manifolds. A great deal of effort aimed at improving the performance of polymer electrolyte membrane (PEM) fuel cells that operate at low temperatures has focused on the development of improved anode catalysts as well as increasing our understanding of the performance and limitations of existing catalyst materials.[3−8] There is clearly a need to develop anode catalysts with improved performance in the presence of electrode-deactivating fuels, such as methanol or hydrogen containing carbon monoxide that is typical of fuels based upon reformed hydrocarbons.

A considerable knowledge base has emerged with respect to the electrochemical characteristics and performance of numerous anode catalysts. Fundamental electrochemical studies have provided detailed information regarding reaction kinetics for the hydrogen oxidation reaction on platinum[9−15] and platinum-based alloys[12,13,16−20] at ambient and higher temperatures. The influence of de-activating species such as carbon monoxide on hydrogen oxidation has also been thoroughly studied[9,21−23] along with more complex oxidation reactions involving methanol,[24−28] formic acid,[29,30] and other fuels.[31,32] Recent

* To whom correspondence should be addressed.

(1) Appleby, A. J.; Foulkes, F. R. *Fuel Cell Handbook;* Van Nostrand Reinhold: New York, 1989.
(2) Larminie, J.; Dicks, A. *Fuel Cell Systems Explained,* 1st ed.; Wiley & Sons: New York, 2000.
(3) Peled, E.; Duvdevani, T.; Aharon, A.; Melman, A. *Electrochem. and Solid State Lett.* **2000**, *3*, 525−528.
(4) Witham, C. K.; Chun, W.; Valdez, T. I.; Narayanan, S. R. *Electrochem. and Solid State Lett.* **2000**, *3*, 497−500.
(5) Ciureanu, M.; Wang, H.; Qi, Z. G. *J. Phys. Chem. B* **1999**, *103*, 9645−9657.
(6) Ciureanu, M.; Wang, H. *J. Electrochem. Soc.* **1999**, *146*, 4031−4040.
(7) Lefebvre, M. C.; Qi, Z. G.; Pickup, P. G. *J. Electrochem. Soc.* **1999**, *146*, 2054−2058.
(8) Baxter, S. F.; Battaglia, V. S.; White, R. E. *J. Electrochem. Soc.* **1999**, *146*, 437−447.
(9) Jambunathan, K.; Shah, B. C.; Hudson, J. L.; Hillier, A. C. *J. Electroanal. Chem.* **2001**, *500*, 279−289.
(10) Markovic, N. M.; Grgur, B. N.; Ross, P. N. *J. Phys. Chem. B* **1997**, *101*, 5405−5413.
(11) Mello, R. M. Q.; Ticianelli, E. A. *Electrochim. Acta* **1997**, *42*, 1031−1039.
(12) Gasteiger, H. A.; Markovic, N. M.; Ross, P. N. *J. Phys. Chem.* **1995**, *99*, 16757−16767.
(13) Gasteiger, H. A.; Markovic, N. M.; Ross, P. N. *J. Phys. Chem.* **1995**, *99*, 8290−8301.
(14) Couturier, G.; Kirk, D. W.; Hyde, P. J.; Srinivasan, S. *Electrochim. Acta* **1987**, *32*, 995−1005.
(15) Clavilier, J.; Durand, R.; Guinet, G.; Faure, R. *J. Electroanal. Chem.* **1981**, *127*, 281−287.
(16) Grgur, B. N.; Markovic, N. M.; Ross, P. N. *J. Electrochem. Soc.* **1999**, *146*, 1613−1619.
(17) Grgur, B. N.; Markovic, N. M.; Ross, P. N. *J. Phys. Chem. B* **1998**, *102*, 2494−2501.
(18) Lin, W. F.; Zei, M. S.; Eiswirth, M.; Ertl, G.; Iwasita, T.; Vielstich, W. *J. Phys. Chem. B* **1999**, *103*, 6968−6977.
(19) Pozio, A.; Giorgi, L.; Antolini, E.; Passalacqua, E. *Electrochim. Acta* **2000**, *46*, 555−561.
(20) Gasteiger, H. A.; Markovic, N. M.; Ross, P. N. *J. Phys. Chem.* **1995**, *99*, 8945−8949.
(21) Markovic, N. M.; Grgur, B. N.; Lucas, C. A.; Ross, P. N. *J. Phys. Chem. B* **1999**, *103*, 487−495.
(22) Breiter, M. W. *J. Electroanal. Chem.* **1980**, *115*, 45−51.
(23) Markovic, N. M.; Lucas, C. A.; Grgur, B. N.; Ross, P. N. *J. Phys. Chem. B* **1999**, *103*, 9616−9623.

10.1021/la010930b CCC: $20.00
Published on Web 11/08/2001

efforts to discover new, more highly active catalysts for the fuel cell anode have focused on developing a greater understanding of and improving catalyst performance in the presence of electrode-deactivating fuels. Platinum-based alloys have been the subject of intense investigation in efforts to develop poison-tolerant catalysts. A number of platinum alloys, including those with ruthenium,[18,27,33−49] molybdenum,[19,50−56] and tin[20,24,31,57−64] have shown promise for enhanced reactivity in these environments.

Ultimately, the search for better fuel cell performance will involve the discovery of new catalyst compositions in addition to continued fundamental studies of these materials to elucidate the origins of enhanced catalyst activity. Given the vast number of potential catalyst combinations available for study, several groups have pursued combinatorial methods for the synthesis and screening of electro-oxidation catalysts.[65−68] These efforts have primarily focused on array-based synthesis and characterization methodologies. Recently, a combinatorial electrochemical study involving the fabrication of an array of multicomponent anode catalysts has identified improved performance for methanol oxidation in a previously untested four-component alloy.[65,67]

In this manuscript we describe a method for catalyst discovery and characterization based upon the construction of a substrate possessing a catalyst gradient combined with a screening tool that achieves in-situ reactivity imaging using the scanning electrochemical microscope (SECM). We describe the fabrication of a gradient in surface coverage of a platinum catalyst created on a catalytically inactive, but electronically conductive indium−tin-oxide (ITO) substrate. A gradient in platinum coverage is created by the application of a nonuniform electric field on an ITO surface[69] during platinum deposition. A linear variation in surface potential produces a nonuniform platinum deposition rate, which results in the formation of a platinum coverage gradient. Catalyst activity is measured locally on the sample surface with the SECM operating in the feedback mode. The SECM depicts a uniformly reactive surface when imaging with a noncatalytic redox probe ($Ru(NH_3)_6^{3+/2+}$). However, significant variations in local reactivity are detected when mapping the surface with a catalytic redox probe (H^+/H_2) designed to reflect reactivity toward the hydrogen oxidation reaction.[9,70] Results clearly identify surface domains expressing a high catalytic activity toward hydrogen oxidation.

Experimental Section

Materials. All experiments were performed in deionized water (18 MΩ, Milli-Q, Millipore Corp., Bedford, MA). Electrolyte solutions contained a combination of Na_2SO_4, H_2PtCl_6, $Ru(NH_3)_6Cl_3$, and H_2SO_4 (Aldrich, Milwaukee, WI), which were used as received. All solutions were deaerated with nitrogen (BOC Gases, Murray Hill, NJ) prior to each measurement.

Substrate Preparation. Gradients in platinum coverage were constructed on indium tin oxide (ITO) substrates (Delta Technologies, Stillwater, MN). Pretreatment of the ITO substrate consisted of cutting one-inch square sections using a diamond scribe followed by sonication in a 50/50 ethanol/water mixture, rinsing with ethanol and then rinsing with copious amounts of deionized water. Substrates were dried thoroughly before use under a stream of dry nitrogen.

A gradient in platinum coverage was created by electrodeposition of platinum onto ITO from a solution containing 10 mM H_2PtCl_6 in 0.1 M Na_2SO_4. The deposition solutions were

(24) Wang, K.; Gasteiger, H. A.; Markovic, N. M.; Ross, P. N. *Electrochim. Acta* **1996**, *41*, 2587−2593.
(25) Kunimatsu, K. *J. Electroanal. Chem.* **1982**, *140*, 205−210.
(26) Beden, B.; Lamy, C.; Bewick, A.; Kunimatsu, K. *J. Electroanal. Chem.* **1981**, *121*, 343−347.
(27) McNicol, B. D.; Short, R. T. *J. Electroanal. Chem.* **1977**, *81*, 249−260.
(28) Lu, G. Q.; Chrzanowski, W.; Wieckowski, A. *J. Phys. Chem. B* **2000**, *104*, 5566−5572.
(29) Lu, G. Q.; Crown, A.; Wieckowski, A. *J. Phys. Chem. B* **1999**, *103*, 9700−9711.
(30) Baldauf, M.; Kolb, D. M. *J. Phys. Chem.* **1996**, *100*, 11375−11381.
(31) Gonzalez, M. J.; Hable, C. T.; Wrighton, M. S. *J. Phys. Chem. B* **1998**, *102*, 9881−9890.
(32) Hable, C. T.; Wrighton, M. S. *Langmuir* **1993**, *9*, 3284−3290.
(33) Rolison, D. R.; Hagans, P. L.; Swider, K. E.; Long, J. W. *Langmuir* **1999**, *15*, 774−779.
(34) Chrzanowski, W.; Kim, H.; Wieckowski, A. *Catal. Lett.* **1998**, *50*, 69−75.
(35) Chu, D.; Gilman, S. *J. Electrochem. Soc.* **1996**, *143*, 1685−1690.
(36) Goodenough, J. B.; Hamnett, A.; Kennedy, B. J.; Manoharan, R.; Weeks, S. A. *J. Electroanal. Chem.* **1988**, *240*, 133−145.
(37) Watanabe, M.; Uchida, M.; Motoo, S. *J. Electroanal. Chem.* **1987**, *229*, 395−406.
(38) Watanabe, M.; Motoo, S. *Electroanal. Chem. and Interfac. Electrochem.* **1975**, *60*, 267−273.
(39) Mukerjee, S.; McBreen, J. *Proceedings of the 2nd International Symposium on New Materials for Fuel Cells and Modern Battery Systems;* Ecole Polytech: Montreal, 1997 pp 548−59.
(40) Davies, J. C.; Hayden, B. E.; Pegg, D. J. *Surf. Sci.* **2000**, *467*, 118−130.
(41) Takasu, Y.; Fujiwara, T.; Murakami, Y.; Sasaki, K.; Oguri, M.; Asaki, T.; Sugimoto, W. *J. Electrochem. Soc.* **2000**, *147*, 4421−4427.
(42) Chrzanowski, W.; Wieckowski, A. *Langmuir* **1998**, *14*, 1967−1970.
(43) Hoster, H.; Iwasita, T.; Baumgartner, H.; Vielstich, W. *J. Electrochem. Soc.* **2001**, *148*, A496-A501.
(44) Crown, A.; Moraes, I. R.; Wieckowski, A. *J. Electroanal. Chem.* **2001**, *500*, 333−343.
(45) Long, J. W.; Stroud, R. M.; Swider-Lyons, K. E.; Rolison, D. R. *J. Phys. Chem. B* **2000**, *104*, 9772−9776.
(46) Lin, W. F.; Iwasita, T.; Vielstich, W. *J. Phys. Chem. B* **1999**, *103*, 3250−3257.
(47) Kabbabi, A.; Faure, R.; Durand, R.; Beden, B.; Hahn, F.; Leger, J. M.; Lamy, C. *J. Electroanal. Chem.* **1998**, *444*, 41−53.
(48) Kauranen, P. S.; Skou, E.; Munk, J. *J. Electroanal. Chem.* **1996**, *404*, 1−13.
(49) Tremiliosi, G.; Kim, H.; Chrzanowski, W.; Wieckowski, A.; Grzybowska, B.; Kulesza, P. *J. Electroanal. Chem.* **1999**, *467*, 143−156.
(50) Zhang, H. Q.; Wang, Y.; Fachini, E. R.; Cabrera, C. R. *Electrochem. and Solid State Lett.* **1999**, *2*, 437−439.
(51) Nakajima, H. *J. Chem. Technol. Biotech.* **1991**, *50*, 555−561.
(52) Nakajima, H.; Kita, H. *Electrochim. Acta* **1990**, *35*, 849−853.
(53) Wang, J.; Nakajima, H.; Kita, H. *Electrochim. Acta* **1990**, *35*, 323−328.
(54) Wang, J. D.; Nakajima, H.; Kita, H. *J. Electroanal. Chem.* **1988**, *250*, 213-217.
(55) Kita, H.; Nakajima, H.; Shimazu, K. *J. Electroanal. Chem.* **1988**, *248*, 181−191.
(56) Grgur, B. N.; Zhuang, G.; Markovic, N. M.; Ross, P. N. *J. Phys. Chem. B* **1997**, *101*, 3910−3913.
(57) Motoo, S.; Okada, T. *J. Electroanal. Chem.* **1983**, *157*, 139−144.
(58) Motoo, S.; Shibata, M.; Watanabe, M. *J. Electroanal. Chem.* **1980**, *110*, 103−109.
(59) Crabb, E. M.; Marshall, R.; Thompsett, D. *J. Electrochem. Soc.* **2000**, *147*, 4440−4447.
(60) Margitfalvi, J. L.; Borbath, I.; Hegedus, M.; Tfirst, E.; Gobolos, S.; Lazar, K. *J. Catal.* **2000**, *196*, 200−204.
(61) Morimoto, Y.; Yeager, E. B. *J. Electroanal. Chem.* **1998**, *444*, 95−100.
(62) Morimoto, Y.; Yeager, E. B. *J. Electroanal. Chem.* **1998**, *441*, 77−81.
(63) Rahim, M. A. A.; Khalil, M. W.; Hassan, H. B. *J. Appl. Electrochem.* **2000**, *30*, 1151−1155.
(64) Grantscharova-Anderson, E.; Anderson, A. B. *Electrochim. Acta* **1999**, *44*, 4543−4550.
(65) Gurau, B.; Viswanathan, R.; Liu, R. X.; Lafrenz, T. J.; Ley, K. L.; Smotkin, E. S.; Reddington, E.; Sapienza, A.; Chan, B. C.; Mallouk, T. E.; Sarangapani, S. *J. Phys. Chem. B* **1998**, *102*, 9997−10003.
(66) Ley, K. L.; Liu, R. X.; Pu, C.; Fan, Q. B.; Leyarovska, N.; Segre, C.; Smotkin, E. S. *J. Electrochem. Soc.* **1997**, *144*, 1543−1548.
(67) Reddington, E.; Sapienza, A.; Gurau, B.; Viswanathan, R.; Sarangapani, S.; Smotkin, E. S.; Mallouk, T. E. *Science* **1998**, *280*, 1735−1737.
(68) Lebl, M. *J. of Combi. Chem.* **1999**, *1*, 3−24.
(69) Terrill, R. H.; Balss, K. M.; Zhang, Y. M.; Bohn, P. W. *J. Am. Chem. Soc.* **2000**, *122*, 988−989.
(70) Zhou, J. F.; Zu, Y. B.; Bard, A. J. *J. Electroanal. Chem.* **2000**, *491*, 22−29.

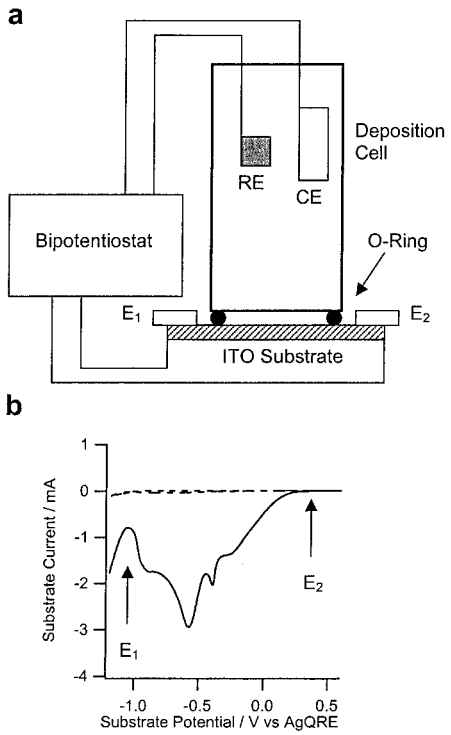

Figure 1. (a) Schematic of deposition method based upon applying a potential gradient along the surface of an indium−tin−oxide (ITO) substrate. A bipotentiostat applies potentials of E_1 and E_2 to two different locations on the same working electrode. (b) Cyclic voltammetry of ITO substrate at a scan rate of 0.1 V s^{-1} in solutions containing 0.1 M Na_2SO_4 (dashed line) and 10 mM H_2PtCl_6 (solid line) in 0.1 M Na_2SO_4 neutralized to a pH of 7. The potentials $E_1 = -1.0$ V and $E_2 = +0.4$ V are shown on the figure.

neutralized to a pH of 7 with saturated NaOH in order to minimize bubble formation during platinum deposition. A surface potential gradient[69] was used to create a nonuniform platinum deposition rate. The potential gradient was achieved by using a bipotentiostat (Model AFDRE, PINE Instrument Company, Grove City, PA) to apply two different potentials to the same working electrode surface. The potentials were applied at different positions by attaching two strips of conductive copper tape across the length of a one-inch square ITO sample separated by approximately 15 mm (Figure 1a). A clamped O-ring cell was attached between the copper strips. During deposition, a wound platinum wire counter electrode and Ag/AgCl quasi-reference electrode (AgQRE) consisting of a AgCl-coated Ag wire were used. The bipotentiostat maintained a linear surface potential gradient by driving current through the ITO surface. ITO films with a resistivity of 10 Ω cm^{-1} were used in order not to overload the bipotentiostat current circuitry. Constant potential values of $E_1 = -1.0$ V and $E_2 = 0.4$ V were applied for a period of approximately two minutes to achieve the platinum gradient depicted in this manuscript.

Scanning Electrochemical Microscope. The scanning electrochemical microscope (SECM) used in this work was similar to that described in the literature.[71−73] Three inchworm translation motors (Model IW-710, Burleigh Instruments, Inc., Fishers, NY) were mounted directly onto one TS-300 (z) and two TS-100 (xy) translation stages configured for three-dimensional orthogonal motion. These stages were mounted directly to a vibration isolation platform. The inchworm motors had a 25-mm range of motion, a mechanical resolution of 4 nm, and optical encoders giving an absolute position reproducibility of 0.5 μm. Position control was achieved with a Series 7000 controller (Burleigh Instruments, Inc., Fishers, NY) interfaced to a GPIB−PCIIA IEEE−488 interface card (National Instruments, Austin, TX). Electrochemical measurements were performed using a bipotentiostat (Model AFDRE, PINE Instrument Company, Grove City, PA) coupled with a high sensitivity current amplifier (Keithley Instruments, Inc., Cleveland, OH), which was used to measure the current at the microelectrode tip. An analog current filter with a 30-ms time constant was used to eliminate the influence line noise on the microelectrode tip response. Data collection was achieved with a multichannel data acquisition board (PCL818, Advantek, Minnetonka, MN) and a custom software program written in Visual Basic.

The electrochemical cell for SECM experiments was made from Teflon with a cell volume of 15 mL. The cell contained slots for reference and counter electrodes, which were pressure-fit with Teflon tape. The substrate electrode was positioned at the bottom of the cell with the electrode surface facing upward and held in place with a droplet of vacuum grease. The plane of the substrate electrode was oriented parallel to the SECM tip scanning direction with a multi-axis tilt stage (Model 39, Newport, Irvine, CA).

During SECM imaging, the substrate was held at a potential of −0.1 V vs AgQRE. The electrochemical activity of the substrate electrode was probed using a solution of 10 mM $Ru(NH_3)_6Cl_3$ in 0.1 M Na_2SO_4. In these experiments, the tip electrode was held at a potential of −0.6 V vs AgQRE, corresponding to the diffusion-limited reduction of $Ru(NH_3)_6^{3+}$. Hydrogen oxidation kinetics were measured in a solution containing 0.01 M H_2SO_4 and 0.1 M Na_2SO_4. In this case, the tip electrode was held at a potential of −1.6 V vs AgQRE, where proton reduction occurs at a diffusion-limited rate. The solutions were deaerated with nitrogen (BOC Gases, Murray Hill, NJ) prior to each measurement.

Tip Electrodes. The microelectrode tips employed in the SECM were fabricated with 25-μm diameter gold wires (Goodfellow, Berwyn, PA) sealed in glass using a technique similar to that described in the literature.[74] The tip of a borosilicate capillary tube (2.0-mm o.d., 0.5-mm i.d., World Precision Instruments, Sarasota, FL) was melted in a methane-air flame until the tip sealed. A 25-μm diameter gold electrode wire was inserted into the capillary tube and sealed in the glass by pulling a vacuum on the open end while simultaneously heating the sealed end of the glass with a coil of Nichrome wire that was resistively heated with a variable transformer (Variac). Once several millimeters of the glass sealed around the wire, heating was stopped and electrical contact was made to the gold wire with a copper contact wire through the open end of the tube using conductive silver epoxy (Epotek, Billerica, MA) and cured in an oven at 100 °C for 1 h. The connecting wire was then fixed into place with 5 Minute Epoxy (ITW Devcon, Danvers, MA) and cured at 100 °C for a period of 4 h. Once sealed, the tip was shaped to achieve a conical geometry with emery paper (600 and 1200 grit). The exposed end was then polished to give a disk-in-plane geometry with a glass-to-metal ratio (R_g) greater than 10:1. Following initial shaping, the electrode tip was polished to a mirror finish using silica polish (1 and 0.05 μm), sonicated in an ethanol/water solution, and rinsed with deionized water before use.

Scanning Electron Microscope. Surface characterization of the substrate was done using a JEOL JXA 840A scanning electron microscope (SEM) with a LaB_6 filament. An accelerating voltage of 20 kV was used in all the SEM experiments. A double-sided copper adhesive tape (3M Electrical Products Division, Austin, TX) was used to provide electrical contact between the conductive portion of the ITO substrate and the sample mount. The surface coverage at different positions on the substrate was estimated by analyzing the SEM micrographs to determine the fraction of Pt to ITO using the image analysis software SCION IMAGE (Scion Corporation, Frederick, MD).

Results and Discussion

Construction of a surface catalyst gradient was achieved by electro-deposition of platinum onto an electronically conductive, but catalytically inactive indium−tin-oxide (ITO) substrate. A bipotentiostat was used to fix the working electrode potential at two different locations on the ITO substrate where E_1 and E_2 were applied. A linear

(71) Kwak, J.; Bard, A. J. *Anal. Chem.* **1989**, *61*, 1794−1799.
(72) Bard, A. J.; Fan, F.-R. F.; Pierce, D. T.; Unwin, P. R.; Wipf, D. O.; Zhou, F. *Science* **1991**, *254*, 68−74.
(73) Mirkin, M. V. *Anal. Chem.* **1996**, *68*, 8, A 177-A 182.
(74) Lee, C. M.; Miller, C. J.; Bard, A. J. *Anal. Chem.* **1991**, *63*, 78−83.

variation in substrate potential was thus created and used to control the local rate of platinum deposition along the surface. In the presence of a surface potential gradient, the platinum deposition rate could be controlled in a reproducible fashion by the magnitude of the local applied potential. Anodic potential values resulted in little or no platinum deposition while cathodic potentials promoted rapid platinum growth. Cyclic voltammetry of the ITO substrate shows the conditions required for platinum deposition (Figure 1b). In the supporting electrolyte solution of 0.1 M Na_2SO_4, the current response reflects the absence of appreciable electrochemical reactions on ITO. Following the addition of 10 mM H_2PtCl_6, several additional features appear in the current response. Deposition of platinum commences during the negative potential scan as indicated by an initial cathodic current at approximately +0.2 V (vs AgQRE). The current magnitude becomes increasingly larger as the electrode potential is scanned in the negative direction, which indicates an increasing rate of platinum deposition. Several additional peaks are observed during the negative potential scan in Figure 1b, whose origins can be ascribed to a combination of platinum reduction, proton adsorption, and bulk proton reduction.

The selection of E_1 and E_2 values determined the extent and range of the surface potential gradient and, thus, the extent of the platinum deposit. For subsequent analysis, a platinum gradient was generated with applied potential values of −1.0 and +0.4 V (vs AgQRE) for E_1 and E_2, respectively. With this selection, very rapid deposition occurred at the position of E_1 while no deposition occurred at E_2. An optical micrograph of this platinum gradient following two minutes of deposition is depicted in Figure 2a. In this image, the ITO substrate is transparent and appears light, while the platinum appears dark. The platinum gradient is confined to a circular region of approximately 12 mm diameter with the perimeter defined by an O-ring seal used during deposition. The highest platinum content appears on the left side of the sample while the lowest platinum content exists on the right. During subsequent analysis of this sample, the region depicted by the dashed box in Figure 2a is examined with surface position indicated by the axis below the figure.

Characterization of the surface structure of the platinum gradient was achieved with a combination of scanning electron and optical microscopy. For the sample depicted in Figure 2a, the platinum deposit consisted of spherical particles of diameters ranging from 0.2 to 0.5 μm following two minutes of deposition. Although the details of the relationship between deposition parameters and particle size will not be addressed in detail here, fine control of the particle size and particle size distribution could be achieved by varying the potential waveform. In particular, the application of a potential pulse program during deposition rather than a constant potential provided conditions where the rate of particle nucleation and growth could be independently adjusted to define the particle size and limit the variation in particle sizes within a sample. Under constant potential deposition conditions shown here, the particle sizes varied, with the more positive potentials leading to larger particles (0.5 μm), and the more negative potentials resulting in smaller particles (0.2 μm). The differences in particle sizes can be explained by considering the competition between particle nucleation and growth at the various surface potential values. At the most negative potentials, nucleation is rapid and continuous, which leads to the formation of many small particles. At less negative potentials, limited nucleation leads to fewer particles that grow to a larger particle size.

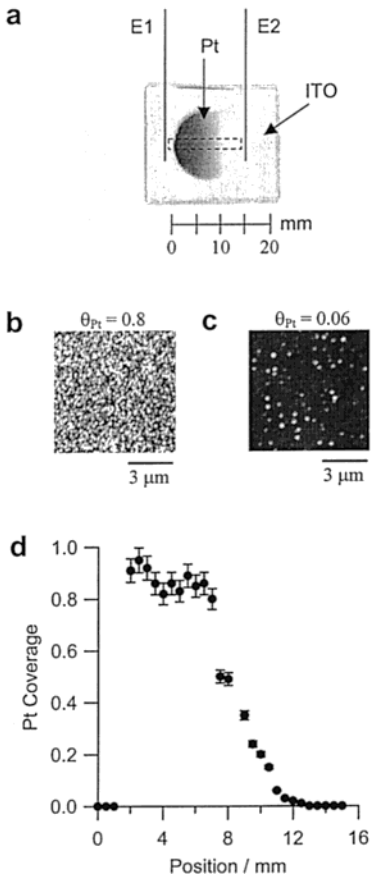

Figure 2. (a) Optical image of platinum coverage gradient created on a circular region on the surface of an ITO substrate. The deposition cell used an O-ring to define the perimeter of deposition. The locations where the potentials E_1 and E_2 were applied are shown. The dashed box reflects the sample region where substrate measurements are taken in subsequent figures and the scale bar reflects the surface axis referred to in the discussion. SEM micrographs taken at a position of (b) 7 mm and (c) 11 mm with platinum coverages of θ_{Pt} 0.8 and 0.06. (d) Summary of platinum surface coverage as a function of distance along the substrate as deduced by image analysis of the SEM micrographs. The error bars reflect the variation in measured surface coverage at each location.

To determine the catalytically active surface area as a function of position on this gradient sample, the platinum surface coverage was estimated. Although the true measure of catalytic activity is given by the number of active catalyst sites per unit surface area, we chose to estimate the activity by determining a ratio of projected surface areas. The coverage was estimated by calculating the ratio of platinum area to total electrode area as a function of position according to

$$\theta_{Pt} = \frac{A_{Pt}}{A_{Pt} + A_{ITO}} \quad (1)$$

where A_{Pt} and A_{ITO} reflect the projected surface areas of Pt and ITO domains as determined from SEM micrographs. A series of high-resolution SEM images of the substrate as a function of spatial position along the platinum gradient were used to determine A_{Pt} and A_{ITO}. Two example SEM images with calculated coverage values of $\theta_{Pt} = 0.8$ (Figure 2b) and $\theta_{Pt} = 0.06$ (Figure 2c) are shown. A series of similar coverage calculations were acquired along the platinum gradient in Figure 2a to construct the surface coverage profile in Figure 2d. Each

Scheme 1. Schematic of Tip−Substrate Interface for SECM Measurements with Noncatalytic Redox Couple $Ru(NH_3)_6^{3+}/Ru(NH_3)_6^{2+}$

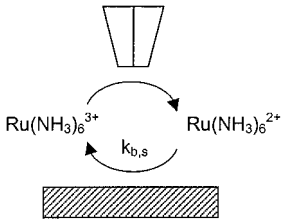

point represents a calculation based upon analysis of a 5000× magnification SEM image taken at that location along the platinum gradient. The error bars reflect the influence of image pixelation on the coverage calculation.

Figure 2d depicts a variation in platinum coverage ranging from zero up to nearly full coverage. Starting from the right side of the sample at 15 mm, the coverage is zero. The coverage then increases starting at 12 mm. Between 11 and 8 mm, the platinum coverage increases and then plateaus between $\theta_{Pt} = 0.8$ and $\theta_{Pt} = 0.95$ at 7 mm. This coverage value is maintained until the edge of the platinum deposit is reached at 2 mm. Although this high coverage region appears uniform in terms of surface coverage, it consists of a thickening platinum layer from right to left. On both the far right (>14 mm) and far left (<2 mm) sides of the sample, the regions blocked by the O-ring during deposition display a zero coverage level and consist of pure ITO.

To locally probe the reactivity of this catalyst gradient for electrochemical and electrocatalytic activity, the SECM was employed. Two different probe molecules were used in the tip reaction to quantify the local reactivity of the substrate surface. To probe the electrochemical activity of the exposed substrate electrode toward a noncatalytic reaction, a simple outer-sphere redox couple ($Ru(NH_3)_6^{3+/2+}$) was used for the tip reaction. In this configuration, the SECM drove the reduction of $Ru(NH_3)_6^{3+}$ at the tip electrode at a diffusion-limited rate.

$$Ru(NH_3)_6^{3+} + e^- \rightarrow Ru(NH_3)_6^{2+} \qquad (2)$$

Under these conditions, the tip reaction achieves a steady-state current in the absence of the substrate ($i_{T,\infty}$) given by the equation

$$i_{T,\infty} = 4nFDCa \qquad (3)$$

where n is the number of electrons, F is Faraday's constant, D is the diffusion coefficient, C is the bulk solution concentration, and a is the tip radius. In an electrolyte solution containing 10 mM $Ru(NH_3)_6Cl_3$ with 0.1 M Na_2SO_4 as the background electrolyte, the tip current measured approximately 27 nA with a 12.5-μm radius tip electrode. The magnitude of this tip current is modified when the tip is placed near a substrate. This results from a combination of mass transfer between tip and substrate and charge-transfer reaction at their surfaces (Scheme 1). In the presence of a nonreactive or insulating substrate, the tip current will diminish with decreasing tip−sample separations (negative feedback) resulting from the blocking of diffusion of the probe molecule to the tip. In the presence of a conducting or electrochemically active substrate that can oxidize the products of the tip reaction, the tip current will increase as it approaches the surface (positive feedback). This behavior is a well-known characteristic of SECM that can be used to deduce the substrate

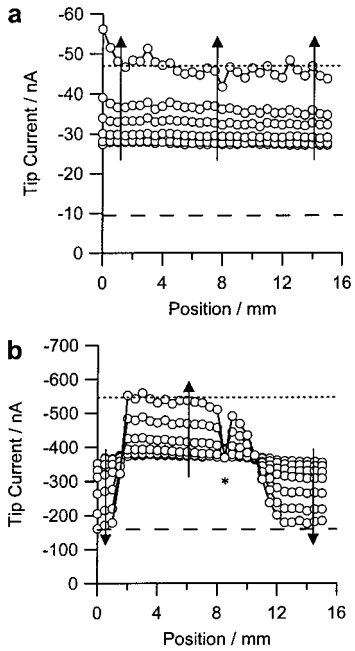

Figure 3. Scanning electrochemical microscope (SECM) line scans along the surface of the platinum gradient on ITO within the region depicted by the dashed box in Figure 2a. (a) Line scans in a solution of 10 mM $Ru(NH_3)_6Cl_3$ and 0.1 M Na_2SO_4 at tip−sample separations of 70, 50, 30, 20, 15, and 10 μm. The tip potential is held at −0.6 V vs AgQRE, where $Ru(NH_3)_6^{3+}$ reduction occurs at a diffusion-limited rate. (b) Line scans in a solution of 0.01 M H_2SO_4 and 0.1 M Na_2SO_4 at tip−sample separations of 105, 85, 65, 45, 25, 15 and 10 μm. The tip potential is held at −1.6 V vs AgQRE, where proton reduction occurs at a diffusion-limited rate. The location denoted as * in (b) possessed a defect in the Pt layer. The substrate potential is −0.1 V vs AgQRE in both (a) and (b). The arrows depict decreasing tip−sample separation. Guidelines depicting the theoretical prediction for (dotted line) pure positive feedback with $k_{b,s} > 1$ cm s^{-1} and (dashed line) pure negative feedback with $k_{b,s} < 0.001$ cm s^{-1} are shown at the distance of closest tip separation in (a) and (b).

rate constant ($k_{b,s}$) for an electrochemical reaction by fitting the approach curve results to a solution of a reaction/diffusion model of the tip−substrate interface.[75,76] The probe reaction of $Ru(NH_3)_6^{3+}$ reduction at the tip electrode results in the oxidation of $Ru(NH_3)_6^{2+}$ as the substrate reaction.

$$Ru(NH_3)_6^{2+} \xrightarrow{k_{b,s}} Ru(NH_3)_6^{3+} + e^- \qquad (4)$$

This probe reaction is quite fast (large $k_{b,s}$) on most electrochemically active surfaces and is independent of the nature of the electrode.

A series of line scans using the $Ru(NH_3)_6^{3+/2+}$ probe reaction were acquired across the platinum coverage gradient (Figure 3a). The line scans were measured at several tip−substrate separations ranging from far from the surface (~100 μm) to very near (~10 μm) along the sample region depicted by the dashed box in Figure 2a. Sample tilt in these data was minimized by careful leveling of the substrate surface using a tilt-stage prior to measurement. At large tip−sample separations (~100 μm), the tip current approaches the value that would be measured in the absence of the substrate ($i_T = i_{T,\infty}$) and

(75) Bard, A. J.; Mirkin, M. V.; Unwin, P. R.; Wipf, D. O. *J. Phys. Chem.* **1992**, *96*, 1861−1868.
(76) Wei, C.; Bard, A. J.; Mirkin, M. V. *J. Phys. Chem.* **1995**, *99*, 16033−16042.

Scheme 2. Schematic of Tip−Substrate Interface for SECM Measurements with Catalytic Redox Couple H^+/H_2

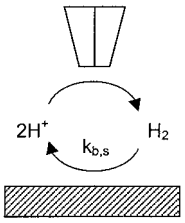

reflects the diffusion-limited current to a disk-in-plane electrode geometry as in eq 3. With decreasing tip−sample separations, the tip current increases uniformly across the entire sample, including over both the platinum gradient and the bare ITO regions. At the smallest tip−sample separations, a variation in tip current appears, which is probably a result of nonuniformity in the substrate topography. However, at all locations on the surface the tip response reflects pure, diffusion-limited positive feedback due to a high substrate rate constant for the reaction depicted in eq 4. As a reference, guidelines depicting the theoretical prediction for (dotted line) pure positive feedback with $k_{b,s} > 1$ cm s^{-1} and (dashed line) pure negative feedback with $k_{b,s} < 0.001$ cm s^{-1} are shown in Figure 3a at the distance of closest tip−sample separation. The pure positive feedback response is consistent with the fact that the entire substrate is electrochemically active and provides a uniformly high rate constant toward $Ru(NH_3)_6^{2+}$ oxidation. Notably, the response is insensitive to the presence of the platinum gradient. Ultimately, the SECM response to this reaction can be used to independently verify the tip−sample separation by fitting the response to the theoretical prediction of pure positive feedback. The only adjustable parameter in this fit is the separation L ($=d/a$).[75,76]

To determine the substrate reactivity toward a catalytic electro-oxidation reaction, a SECM probe reaction that is sensitive to catalytic activity was used. Specifically, the hydrogen oxidation reaction was probed by using the H^+/H_2 redox couple.[9,70] Protons were reduced at the tip electrode at a diffusion-limited rate.

$$2H^+ + 2e^- \rightarrow H_2 \qquad (5)$$

With this tip reaction, hydrogen produced by the tip diffuses to the substrate and can be oxidized back to protons (Scheme 2).

$$H_2 \xrightarrow{k_{b,s}} 2H^+ + 2e^- \qquad (6)$$

Protons produced at the substrate can then diffuse back to the tip to increase the tip current and provide a positive tip−substrate feedback response. The magnitude of this positive feedback reflects the rate constant for hydrogen oxidation at the substrate electrode ($k_{b,s}$).[70,75−77]

A series of line scans at various tip−sample separations using proton reduction as the tip reaction were acquired across the platinum gradient. These data are illustrated in Figure 3b. The line scans were acquired over the same sample region and range of tip−sample separations as those depicted in Figure 3a. At large tip−sample separations (~100 μm), the tip current is uniform and approaches a value of 360 nA, which is approximately equal to the current measured in the absence of the substrate electrode and corresponds to the value predicted in eq 3. With decreasing tip−sample separations, the tip response begins to change nonuniformly over the sample surface, which is in contrast to the behavior for the noncatalytic $Ru(NH_3)_6^{3+/2+}$ probe shown in Figure 3a. At regions to the far left and far right of the sample, the tip current decreases as it approaches the substrate surface. These regions correspond to the bare ITO surface and the decrease in tip current reflects negative feedback for the hydrogen oxidation reaction. In fact, the rate constant for hydrogen oxidation is nearly zero on ITO so the tip response corresponds to almost pure blocking of proton diffusion to the tip.

The tip response over the bare ITO regions contrasts to that observed over the platinum-coated regions. Over the platinum-coated ITO, the tip response varies from negative feedback to positive feedback depending upon the tip position along the surface. At the far right side of the sample, the tip current decreases with decreasing tip−sample separation. At 12 mm and higher, this decrease in tip current reflects pure negative feedback. As a reference, guidelines depicting the theoretical prediction for pure positive feedback with $k_{b,s} > 1$ cm s^{-1} (dotted line) and pure negative feedback with $k_{b,s} < 0.001$ cm s^{-1} (dashed line) are shown in Figure 3b at the distance of closest tip−sample separation. The negative feedback response is due to the low activity toward hydrogen oxidation for the very low coverage ITO sample regions. At sample positions to the left of 12 mm, the tip current decreases less severely with sample approach. This reflects an increasing rate constant for hydrogen oxidation that is coincident with the increase in platinum coverage at this region of the sample (Figure 2d). Between 12 mm and 7 mm, the tip response transforms from negative to positive feedback. The increasing positive feedback in this sample region indicates an increasing rate of hydrogen oxidation due to the surface transition from catalytically inactive ITO to catalytically active platinum regions. Further excursions in the tip position from 7 mm to 2 mm maintains a nearly pure positive feedback response, which reflects a very high rate constant for hydrogen oxidation on the high coverage platinum surface.

To quantify the variation in reactivity of the platinum gradient toward the hydrogen oxidation reaction, the results from Figure 3b were used to determine the rate constant as a function of surface position. Each line scan in Figure 3b represents a series of equal-spaced, steady-state tip current measurements at a fixed separation. These measurements can be used to generate a tip−substrate approach curve by taking the tip current at each position along the gradient and converting the current and tip−substrate separation to a normalized scale. The tip current (i_T) is divided by the value at infinite separation ($i_{T,\infty}$) while the tip−sample separation (d) is divided by the tip radius (a). The absolute separation between tip and sample for these points has been adjusted by assuming the results from Figure 3a reflect pure positive feedback and calculating the tip−sample separation based upon fitting these results to a theoretical working curve.[75,76] The approach curves measured for the hydrogen oxidation reaction along the platinum catalyst gradient are depicted in Figure 4. As was done in Figure 3, reference guidelines are shown for approach curves based upon the theoretical prediction for pure positive (dotted line) and pure negative feedback (dashed line). The upper curve in the data represents that measured at 2 mm and corresponds to a high coverage platinum region with essentially pure positive feedback. The very lowest curve in Figure 4 represents the data acquired at 15 mm where the platinum

(77) Mirkin, M. V. *Mikrochim. Acta* **1999**, *130*, 127−153.

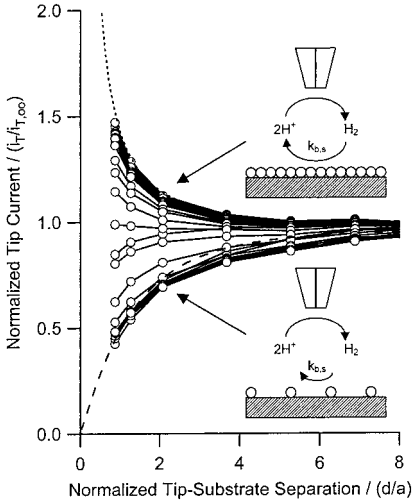

Figure 4. Approach curves adapted from the results for hydrogen oxidation. The data are re-plotted from Figure 3b by taking the tip current at each position along the gradient and converting the current and tip−substrate separation to a normalized scale. The tip current (i_T) has been divided by the value at infinite separation ($i_{T,\infty}$) while the tip−sample separation (d) has been divided by the tip radius (a). Lines corresponding to the theoretical prediction for (dotted line) pure positive feedback with $k_{b,s} > 1$ cm s^{-1} and (dashed line) pure negative feedback with $k_{b,s} < 0.001$ cm s^{-1} are shown for reference. The inset schematics depict the tip−sample interface in the presence of high (upper) and low (lower) surface coverage of platinum. The approach curves corresponding to these conditions are identified by the arrows.

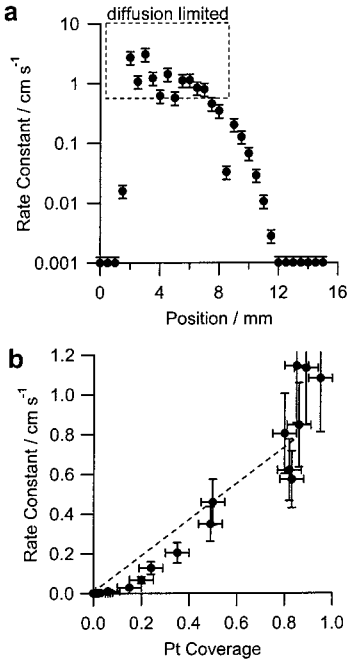

Figure 5. (a) Summary of electrochemical rate constant values for hydrogen oxidation as a function of surface position as deduced by fitting the experimental approach curves from Figure 4 to a theoretical model.[76] The error bars reflect the variation in model results and are attributable to an uncertainty in the substrate position of approximately ±2.5 μm. The dashed box reflects an approximate upper limit in the measurable rate constant where the response is diffusion limited. (b) Rate constant values plotted as a function of surface coverage. The dashed line represents a linear increase in rate with coverage according to eq 7 in the text.

coverage is zero. This response reflects pure negative feedback and a rate constant with a value of essentially zero for hydrogen oxidation. The intermediate curves represent positions intermediate between 0 and 15 mm on the platinum gradient. These results can be fit to a theoretical working curve according to the standard procedure[70,75−77] in order to extract the rate constant for the hydrogen oxidation reaction as a function of surface position.

A series of rate constant values were determined with the data illustrated in Figure 4 and are depicted in Figure 5a as a function of surface position. It is important to note that these rate constants reflect values for hydrogen oxidation that are based upon a local geometric region of the substrate surface rather than a value based upon the number of catalyst sites. Nevertheless, these data reflect the local surface reactivity for hydrogen oxidation. The accuracy of these rate constants is limited to values between 0.001 and 1 cm s^{-1}. Rate constants equal to or less than 0.001 cm s^{-1} are below the measurable limit for fitting SECM approach curves and display a behavior that is equivalent to pure negative feedback. Rate constants equal to or greater than approximately 1 cm s^{-1} are consistent with diffusion-controlled positive feedback. Measuring accurate rate constant values beyond this range with SECM is limited (in our hands) due to tip size and tip−substrate geometry effects. However, a recent study using a SECM tip in combination with an impinging jet suggests that the upper limit can be extended.[78,79] Notably, the range reported here is larger than the typical rate constant values accessible with rotating disk techniques.

The trend in the measured rate constant values shown in Figure 5a is consistent with the trend in platinum coverage in Figure 2d. At positions possessing platinum-free ITO (<2 mm and >12 mm), the measured rate constant is effectively zero. As the sample is traversed from the right to the left, the rate constant for hydrogen oxidation increases. The first measurable increase is observed at 12 mm, where the platinum coverage first increases above zero (Figure 2d). The rate constant then increases significantly between 12 and 7 mm. At 7 mm, the rate constant approaches 1 cm s^{-1} and is effectively diffusion-limited until the bare ITO region is again reached at 2 mm. Comparing this result to the coverage data displayed in Figure 2d suggests that the hydrogen oxidation rate is increasing in coincidence with the increase in platinum coverage. The point at which the rate constant becomes high enough for the response to become diffusion-limited corresponds to the substrate reaching a limiting coverage of about 0.9.

Although both the platinum coverage and hydrogen oxidation rate constant are nonlinear functions of position in this sample, it is expected that they should be linearly related to each other. The rate constant values versus position from Figure 5a and the coverage versus position from Figure 2d are combined in Figure 5b to show the rate constant value as a function of platinum coverage. A dashed line is added to depict a linear increase in rate constant with coverage according to

$$k_{\text{measured}} = k_{\text{Pt}}\theta_{\text{Pt}} \qquad (7)$$

where k_{measured} is the experimentally measured rate constant, k_{Pt} is the rate constant on full coverage Pt, and θ_{Pt} is the platinum coverage. The experimental values do a reasonable job in following this linear relationship between rate constant and coverage. At low coverage

(78) Macpherson, J. V.; Jones, C. E.; Unwin, P. R. *J. Phys. Chem. B* **1998**, *102*, 9891−9897.
(79) Macpherson, J. V.; Unwin, P. R. *Anal. Chem.* **1998**, *70*, 2914−2921.

values, the experimentally measured rate drops slightly below this straight-line dependence. This behavior can be explained by the fact that the SEM images of this low coverage region depict slightly larger platinum cluster sizes than those observed in the high coverage region. The larger particle size would produce a smaller surface area per volume and potentially a lower effective oxidation rate. In addition, at low surface coverage the small size of the SECM tip might allow nonuniform sampling of the surface. However, it is expected that this latter effect would lead to both over and under-estimates of the rate and, thus, cancel out in average. At coverage values above $\theta_{Pt} = 0.8$, the rate constants also deviate from the straight-line dependence. This is likely the result of the inaccuracy of the measured rate constant values as they approach and exceed 1 cm s^{-1}.

Conclusions

In this work we have demonstrated a combinatorial electrochemical method for catalyst preparation and screening based upon the construction of a surface catalyst gradient combined with reactivity mapping using a scanning electrochemical microscope. The novelty of this gradient preparation technique is that it allows the construction of a continuous variation in an important catalytic parameter in a single sample. This work focused on the construction of a coverage gradient, but we are extending this work to the formation of gradients in other parameters such as particle size and composition, which are particularly important in the search for improved, multicomponent fuel cell catalysts. The reactivity screening method utilized here has a number of promising features and several advantages over array-based strategies. The SECM can be used to quantitatively map the rate constant for the hydrogen oxidation reaction. In addition, the detection of protons can be used to quantify the rate of a number of oxidative de-hydrogenation reactions, including the oxidation of methanol and formic acid. Also, the ability to indirectly measure oxidation reactions with this electrochemical imaging method eliminates the need for the complex wiring and sample preparation required for array-based methods.

Acknowledgment. The authors would like to acknowledge the Office of Naval Research (Young Investigator Program), the Camille and Henry Dreyfus Foundation (New Faculty Award), and the donors of the Petroleum Research Fund as administered by the American Chemical Society for partial funding of this work.

LA010930B